Why Fourier Mode Analysis in Time is Different when Studying Schwarz Waveform Relaxation

Martin J. Gander, Véronique Martin

Abstract

Schwarz waveform relaxation methods are Schwarz methods applied to evolution problems. Like for steady problems, they are based on an overlapping domain decomposition of the spatial domain, and an iteration which only requires subdomain solutions, now in space-time, to get better and better approximations of the global, monodomain solution. Fourier analysis has been used to study the convergence of both Schwarz and Schwarz waveform relaxation methods. We show here that their convergence is however quite different: for steady problems of diffusive type, Schwarz methods converge linearly, which is also well predicted by Fourier analysis. For a time dependent heat equation however, the Schwarz waveform relaxation algorithm first has a rapid convergence phase, followed by a slow down, and eventually convergence increases again to become superlinear, none of which is predicted by classical Fourier analysis. Introducing a new Fourier analysis combined with kernel estimates, we can explain this behavior for the heat equation. We then generalize our approach to the case of advection reaction diffusion problems. We illustrate all our results with numerical experiments.

Keywords: Fourier analysis in time, Schwarz Waveform Relaxation

1. Introduction

Schwarz Methods and Schwarz Waveform Relaxation methods are powerful algorithms to approximate solutions of partial differential equations (PDEs) on parallel computers, see e.g. [1, 2, 3, 4, 5, 6, 7, 8, 9, 10] and references therein. They are based on a decomposition of the computational domain into subdomains, and an iteration that only computes subdomain solutions, and which converges to the solution on the entire computational domain. Schwarz methods were invented by Hermann Amandus Schwarz [11] in order to prove existence and uniqueness of solutions for the Laplace problem on general domains. They became a computational tool to solve elliptic partial differential equations with Miller [12], and then mainstream parallel solvers with the seminal work of Lions [13] and Dryja and Widlund [14]; for a historical review, see [15, 16]. Schwarz waveform relaxation methods are for solving time dependent partial differential equations, and their name goes back to the invention

of waveform relaxation methods for circuit simulation in [17]. They are also based on a decomposition of the computational domain into subdomains and a subdomain iteration, but now problems in space and time are solved in each subdomain [18, 2, 3, 19]. Schwarz waveform relaxation methods were also instrumental in the development of optimized transmission conditions between subdomains, leading to optimized Schwarz (waveform relaxation) methods [20, 7], even though first optimized transmission conditions can already be found in [21], see [22] for a more complete literature review. First analyses for these methods for parabolic problems were based on maximum principle arguments, see e.g. [3], but more detailed information on the convergence mechanisms can be obtained using Fourier analysis [23], which was essential for the optimization of transmission conditions, see [22] for elliptic problems, [7, 8, 24, 10] for parabolic problems, and [5, 25] for hyperbolic problems. Schwarz waveform relaxation methods are one of four classes of space-time parallel methods, which have been intensively researched over the past two decades in the context of PinT (parallel in time) methods, see [26] for a historical review, and [27] for recent applications.

In [3, 2] and [23], two different bounds for the convergence of Schwarz waveform relaxation were proved when applied to the heat equation on the spatial domain $\Omega :=(-a, a)$ split into two equal subdomains Ω_j with an overlap L: the error e_j^n on subdomain Ω_j at iteration n satisfies the *linear bound* $\|e_j^n(0,\cdot)\|_{L^\infty} \leq \left(\frac{a-L}{a+L}\right)^n \|e_j^0(0,\cdot)\|_{L^\infty}$ using maximum principle arguments, which is sharp for long time windows, and the *superlinear bound* $\|e_j^n(0,\cdot)\|_{L^\infty} \leq \operatorname{erfc}(\frac{nL}{2\sqrt{\nu T}})\|e_j^0(0,\cdot)\|_{L^\infty}$ using detailed heat kernel estimates, which is sharp for short time windows , and we will call these the linear and superlinear bounds in what follows. More insight on the convergence behavior can be obtained using Fourier analysis, both for Schwarz methods applied to elliptic problems, and Schwarz waveform relaxation methods applied to parabolic and hyperbolic problems. But the convergence mechanisms for these two classes of methods differ: Schwarz methods for elliptic problems converge linearly, already shown by Schwarz himself [11], and Schwarz waveform relaxation methods for parabolic problems obey both the linear and superlinear convergence estimates above. We show in Figure 1 on the left how the error decreases as the iteration of the Schwarz algorithm progresses when applied to a screened Laplace problem $(\eta - \Delta)u = f$. We see that after a rapid initial phase, the convergence is linear: every new iteration gives the same error decay as the previous one, which is well predicted by Fourier analysis shown in red in Figure 1, see Section 2 for more details. On the right in Figure 1 we show how the error decreases as the iteration of the Schwarz waveform relaxation algorithms progresses when applied to a heat equation $\partial_t u = \Delta u + f$, see Section 3 for more details. We clearly see that the convergence behavior is much more complicated in the time dependent case, compared to the steady case: there is an initial phase of rapid convergence, followed by a significant slow down, and then convergence speeds up again and eventually becomes superlinear. The Fourier bound shown in red in Figure 1 on the right does not seem to well capture any phase of the convergence. Our

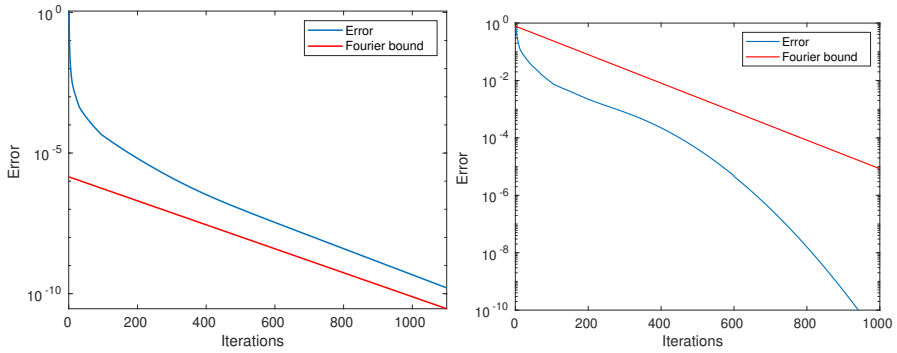

Figure 1: Decay of the error as function of the iteration for a Schwarz algorithm applied to a screened Laplace equation (left) and a Schwarz waveform relaxation algorithm applied to a heat equation (right).

goal here is to understand this difference in convergence behavior, since Fourier analysis leads to a very similar convergence factor in both the steady and time dependent cases, and we want to connect the Fourier bound with the linear and superlinear bounds from [2] and [23].

Our paper is structured as follows: in Section 2, we review Fourier mode analysis for Schwarz methods when applied to the screened Laplace equation, which leads to the linear convergence observed in Figure 1 on the left. In Section 3, we present a new Fourier mode analysis combined with kernel estimates for when Schwarz waveform relaxation is applied to the heat equation, which allows us to explain where the different convergence behaviors observed in Figure 1 on the right come from. In Section 4, we generalize our analysis of the complicated convergence behavior observed in Figure 1 (right) to the advection-reaction-diffusion equation. We give conclusions and an outlook on future work in Section 5.

2. Fourier analysis for Schwarz applied to stationary PDEs

We consider for our stationary PDE the screened Laplace equation

$$\tilde{\mathcal{L}}u := \eta u - \triangle u = f, \quad \text{in } \Omega := \mathbb{R}^2, \tag{1}$$

with $\eta > 0$. If the domain Ω is split into the two overlapping subdomains $\Omega_1 := (-\infty, L) \times \mathbb{R}$ and $\Omega_2 := (0, +\infty) \times \mathbb{R}$, where Ł > 0 is the overlap parameter, then the classical alternating Schwarz algorithm solves for iteration index $k = 1, \ldots$

$$\begin{array}{ll} \tilde{\mathcal{L}}u_1^k = f & \text{on } (-\infty, L) \times \mathbb{R}, \\ u_1^k(L, \cdot) = u_2^{k-1}(L, \cdot) & \text{on } \mathbb{R}, \end{array} \qquad \begin{array}{ll} \tilde{\mathcal{L}}u_2^k = f & \text{on } (0, +\infty) \times \mathbb{R}, \\ u_2^k(0, \cdot) = u_1^k(0, \cdot) & \text{on } \mathbb{R}. \end{array} \tag{2}$$

The error $e_j^k := u - u_j^k$, $j = 1, 2$ satisfies by linearity the same algorithm (2) but with right hand side $f = 0$. If the initial error is a pure sine signal on the

interface, $e_2^0(L,y) := \sin(\lambda y)$, then the errors for each iteration $k = 1, 2, \ldots$ can be obtained by a direct computation to be

$$\begin{aligned} e_1^k(x,y) &= e^{-(2k-1)L\sqrt{\eta+\lambda^2}} e^{\sqrt{\eta+\lambda^2}x} \sin(\lambda y), \\ e_2^k(x,y) &= e^{-(2k-1)L\sqrt{\eta+\lambda^2}} e^{-\sqrt{\eta+\lambda^2}x} \sin(\lambda y), \end{aligned} \tag{3}$$

and we thus obtain

$$e_1^k(0,y) = e^{-(2k-1)L\sqrt{\eta+\lambda^2}} \sin(\lambda y) =: \rho(\lambda)^{2k-1} \sin(\lambda y), \tag{4}$$

which means that at each iteration the initial sine error is contracted by the convergence factor $\rho(\lambda)$. This result is consistent with the definition of the convergence factor in [22] which was obtained by a Fourier transform in the y direction with Fourier variable ω,

$$\rho_F(\omega) := \sqrt{\frac{\hat{e}_1^{k+1}(0,\omega)}{\hat{e}_1^k(0,\omega)}} = e^{-L\sqrt{\eta+\omega^2}}, \tag{5}$$

where $\hat{e}_1^k(x,\omega) = \hat{e}_2^0(L,\omega) e^{-(2k-1)L\sqrt{\eta+\omega^2}} e^{\sqrt{\eta+\omega^2}x}$ is the Fourier transform of e_1^k. This means that $\hat{e}_1^k(0,\omega) = \rho_F(\omega)^{2k-1} \hat{e}_1^1(0,\omega)$, and $\rho_F(\omega)$ actually describes the convergence speed of the algorithm when the frequency ω is introduced.

There is an interesting graphical interpretation of this convergence process which will be very useful later to understand the main difference for time dependent problems: when introducing as initial error the pure sine signal $e_2^0(L,y) := \sin(\lambda y)$, the error at iteration k can in fact be given in closed form, $e_1^k(0,y) = v((2k-1)L, y)$, where v is the bounded solution of $\tilde{\mathcal{L}} v = 0$ on $(0, +\infty) \times \mathbb{R}$ with the boundary condition $v(0,y) = \sin(\lambda y)$. This is because in the Schwarz algorithm (2) for zero right hand side for the error, the left and right subdomain problems become by symmetry the same, one just solving on Ω_1 in the negative x direction, and the other solving on Ω_2 in the positive x direction, and thus these solutions can be concatenated. We show in Figure 2 on the left the level sets of $v(x,y)$ as a function of x and y for $\lambda = 3\pi$. We can see how the sine error mode is contracted by $\rho(\lambda)$ when x grows, which is also illustrated in Figure 2 on the right. The Fourier analysis used in [22] is thus perfectly well adapted to study the convergence of a pure sine error frequency injected as initial guess into the Schwarz algorithm applied to an elliptic problem, and the slope of the linear convergence observed in Figure 1 on the left corresponds precisely to the convergence of the error frequency which converges the most slowly.

We solved for this experiment on the left the Laplace equation on the domain $(0,16)\times(0,16)$ decomposed into $\Omega_1 := (0, 8.025)\times(0,1)$ and $\Omega_2 := (8,16)\times(0,1)$, used a standard 5 point finite difference scheme with spatial steps $\Delta x = \Delta y = \frac{16}{3200} = 0.005$, and initialized the Schwarz algorithm with random numbers in $(-1,1)$.

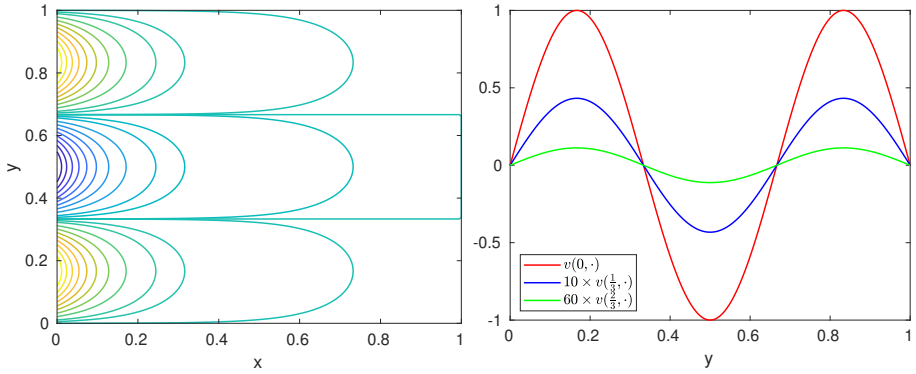

Figure 2: Left: level sets of the solution of the Laplace equation in the (x, y)-plane when $v(0, y) = \sin(3\pi y)$. Right: slices of the scaled solution (for better visibility) at $x = 0$, $x = \frac{1}{3}$ and $x = \frac{2}{3}$.

3. Kernel Fourier Analysis for Schwarz Waveform Relaxation

For time dependent equations we consider as our model problem the heat equation on the domain $\Omega := \mathbb{R}$,

$$\begin{aligned} \mathcal{L}u := \frac{\partial u}{\partial t} - \nu \frac{\partial^2 u}{\partial x^2} = f \quad & \text{in } \Omega \times (0, T), \\ u(\cdot, 0) = 0 \quad & \text{in } \Omega, \end{aligned}$$

where $\nu > 0$ is a positive parameter and $T \in (0, \infty)$. We decompose the space-time domain $\Omega \times (0, T)$ into two space-time subdomains $\Omega_1 \times (0, T)$ and $\Omega_2 \times (0, T)$, with $\Omega_1 := (-\infty, L)$ and $\Omega_2 := (0, \infty)$, where $L > 0$ is again the overlap parameter. The alternating Schwarz waveform relaxation algorithm then computes for iteration index $k = 1, 2, \ldots$

$$\begin{array}{llll} \mathcal{L}u_1^k = f & \text{on } (-\infty, L) \times (0, T), & \mathcal{L}u_2^k = f & \text{on } (0, +\infty) \times (0, T), \\ u_1^k(L, \cdot) = u_2^{k-1}(L, \cdot) & \text{on } (0, T), & u_2^k(0, \cdot) = u_1^k(0, \cdot) & \text{on } (0, T), \\ u_1^k(\cdot, 0) = u_0 & \text{on } (-\infty, L), & u_2^k(\cdot, 0) = u_0 & \text{on } (0, +\infty). \end{array} \tag{6}$$

The error $e_j^k := u - u_j^k$, $j = 1, 2$ satisfies by linearity again the same algorithm (6) but with right hand side $f = 0$ and initial condition $u_0 = 0$.

We can again interpret the Schwarz waveform relaxation algorithm graphically, since the subdomain solutions in (6) have the same symmetry with respect to the x variable as in the screened Laplace case. In Figure 3 on the left we show the level sets of the solution of the heat equation when it is solved with the boundary condition $v(0, t) = \sin(3\pi t)$ and zero initial condition, $u_0(x) = 0$. We see that in contrast to the screened Laplace case in Figure 2 the sine is not only contracted, it is also transported in time and distorted for small t, see also Figure 3 on the right. The sine function is not an eigenfunction of the Schwarz waveform relaxation iteration, and this is the main reason that the

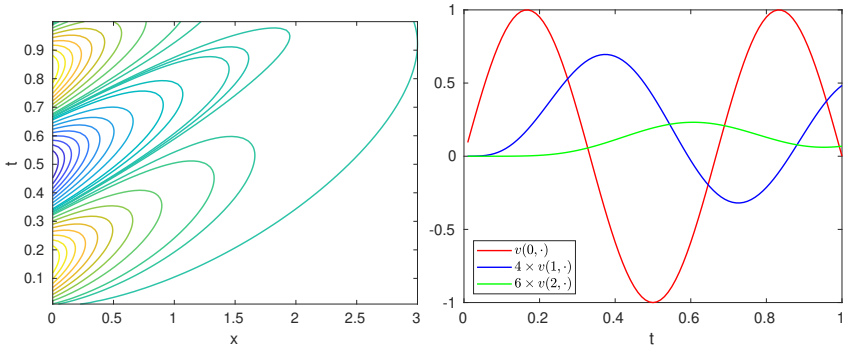

Figure 3: Left: level sets of the solution of the heat equation in the (x,t)-plane when $v(0,t) = \sin(3\pi t)$. Right: slices of the scaled solution at $x = 0$, $x = 1$ and $x = 2$.

convergence of the Schwarz waveform relaxation algorithm is so different from the convergence of the Schwarz algorithm, as we have seen in Figure 1: while for the screened Laplace equation the convergence is linear as indicated by the Fourier analysis, for the heat equation there are three distinct phases for the convergence, which are generated by the transport and distortion of the sine function.

To understand in detail the error decay of the Schwarz waveform relaxation algorithm, we use now Laplace transforms, which are the pendent to Fourier transforms for initial value problems. The Laplace transform of a function $f \in L^1(\mathbb{R})$ satisfying $|f(t)| \leq Ce^{\alpha t}$, $C > 0$ and α constants, is defined by[1]

$$\mathcal{F}(f)(s) = \int_0^{+\infty} f(t)e^{-st}dt, \quad \Re(s) \geq \alpha,$$

where $s := \sigma + i\omega$, $\sigma, \omega \in \mathbb{R}$. If we initialize the algorithm (6) for the error with an initial error at the interface $e_2^0(L,t) = g(t)$, then the Laplace transform of the heat equation in the subdomain Ω_j is $s\hat{e}_j^{k+1} - \nu\frac{\partial^2 \hat{e}_j^{k+1}}{\partial x^2} = 0$, and the solutions are for $k \geq 1$ given by

$$\begin{aligned} \hat{e}_1^k(x,s) &= \hat{g}(s)e^{-(2k-1)\sqrt{\frac{s}{\nu}}L}e^{\sqrt{\frac{s}{\nu}}x}, \\ \hat{e}_2^k(x,s) &= \hat{g}(s)e^{-(2k-1)\sqrt{\frac{s}{\nu}}L}e^{-\sqrt{\frac{s}{\nu}}x}, \end{aligned} \tag{7}$$

similar to the Fourier mode analysis of the screened Laplace case in (3). This leads to the complex convergence factor, see e.g. [28],

$$\rho_L(\omega) := \sqrt{\frac{\hat{e}_1^{k+1}(0,s)}{\hat{e}_1^k(0,s)}} = e^{-\sqrt{\frac{\sigma+i\omega}{\nu}}L}, \tag{8}$$

[1] We still use the Fourier transform symbol $\mathcal{F}$ here to denote the Laplace transform.

which looks very similar to the convergence factor for the screened Laplace case in (5), and thus suggests similar linear convergence.

If we introduce however the kernel function

$$K(x,t) = \frac{x}{2\sqrt{\pi}} \frac{e^{-\frac{x^2}{4t}}}{t^{3/2}}, \tag{9}$$

and use the Laplace transform formula

$$e^{-x\sqrt{s}} = \mathcal{F}(t \to K(x,t))(s), \tag{10}$$

we can obtain a closed form expression of the error at the $k-$th iterate, $k \geq 1$, in terms of the initial guess g on the interface: from

$$\hat{e}_1^k(0,s) = \hat{g}(s) e^{-(2k-1)L\sqrt{\frac{s}{\nu}}} = \hat{g}(s)\mathcal{F}(t \to K((2k-1)\frac{L}{\sqrt{\nu}}, t), \tag{11}$$

we obtain by back-transforming (11) the convolution product

$$e_1^k(0,t) = \int_0^t g(t-\tau) K((2k-1)\frac{L}{\sqrt{\nu}}, \tau) d\tau. \tag{12}$$

This result holds in particular for the pure sine initial guess $g(t) := \sin(\lambda t)$, and shows that the error is clearly not anymore a sine that is contracted by $\rho_L(\lambda)$.

We now study in detail the behavior of the error given by the convolution formula (12). We split the integral into two parts,

$$z_1(x,t;\lambda) := \int_0^{+\infty} \sin(\lambda(t-\tau)) K(x,\tau) d\tau,$$
$$z_2(x,t;\lambda) := -\int_t^{+\infty} \sin(\lambda(t-\tau)) K(x,\tau) d\tau,$$

then the error is given by the sum

$$e_1^k(0,t) = z_1((2k-1)\frac{L}{\sqrt{\nu}}, t; \lambda) + z_2((2k-1)\frac{L}{\sqrt{\nu}}, t; \lambda). \tag{13}$$

We will show in Lemma 1 that the first term z_1 can be explicitly computed: it is a sine which is contracted by the Fourier convergence factor (8), and this shows precisely to which extend the linear convergence of the stationary case also appears in the evolution case. We next explain the behavior of the second term z_2: the convergence factor corresponding to z_2 can also be computed, see Theorem 2, and for large time it can even be neglected for the study of Schwarz waveform relaxation methods, see Theorem 1.

To prove these results, we use the symmetry in the x coordinate of the heat equation: let v be the bounded solution of the homogeneous heat equation $\mathcal{L}v = 0$ on $(0,+\infty)\times(0,+\infty)$ with the initial condition $v(\cdot,0) = 0$ and the boundary condition $v(0,\cdot) = g$. The Laplace transform of the error in the Schwarz

waveform relaxation algorithm (6) then satisfies $\hat{e}_1^k(0,s) = \hat{g}(s)e^{-(2k-1)\sqrt{\frac{s}{\nu}}L} = \hat{v}((2k-1)L,s)$ and $\hat{e}_2^k(L,s) = \hat{v}(2kL,s)$. As a consequence, to obtain the error of the Schwarz waveform relaxation algorithm at iteration k, it suffices to evaluate v at $x = (2k-1)L$ for $e_1^k(0,\cdot)$ and at $x = 2kL$ for $e_2^k(L,\cdot)$, which explains the importance of the level sets of v we have observed in Figure 3 for the performance of the algorithm.

The next theorem shows that the error of the Schwarz waveform relaxation algorithm behaves as predicted by the Laplace analysis for large time for a given Fourier mode λ.

Theorem 1. *Let $T = +\infty$. If the Schwarz waveform relaxation algorithm (6) is initialized with the pure sine frequency error $e_2^0(L,t) = \sin(\lambda t)$, then for large time $t >> 1$, we have*

$$e_1^k(0,t) = |\rho_L(\lambda)|^{2k-1}\sin(\lambda t - (2k-1)L\sqrt{\frac{\lambda}{2\nu}}) + \mathcal{O}(\frac{1}{t^{1/2}}),$$

with an analogous expression for e_2^k.

Before proving this theorem, we give a more accurate result when the algorithm is applied to a single frequency λ. The convergence speed is the result of a competition between the Fourier convergence factor $\rho_L(\lambda)^{2k-1}$ and the term z_2. The Fourier convergence factor gives linear convergence, while the second term decreases as described in the next theorem.

Theorem 2. *Let $T = +\infty$. If the Schwarz waveform relaxation algorithm (6) is initialized with the pure sine frequency $e_2^0(L,t) = \sin(\lambda t)$ then the error is given by*

$$e_1^k(0,t) = |\rho_L(\lambda)|^{2k-1}\sin(\lambda t - (2k-1)L\sqrt{\frac{\lambda}{2\nu}}) + z_2((2k-1)\frac{L}{\sqrt{\nu}},t;\lambda),$$

where z_2 satisfies for large frequency λ

$$z_2((2k-1)\frac{L}{\sqrt{\nu}},t;\lambda) = \frac{1}{\lambda}K((2k-1)\frac{L}{\sqrt{\nu}},t) + \mathcal{O}(\frac{1}{\lambda^3}),$$

and for large iteration k

$$\|z_2((2k+1)\frac{L}{\sqrt{\nu}},\cdot;\lambda)\|_{L^\infty(0,+\infty)} \sim (\frac{2k-1}{2k+1})^2\|z_2((2k-1)\frac{L}{\sqrt{\nu}},\cdot;\lambda)\|_{L^\infty(0,+\infty)}.$$

An analogous result also holds for e_2^k.

The proof of Theorem 1 and Theorem 2 relies on two lemmas. The first lemma gives an explicit formula for z_1.

Lemma 1. *For $x > 0$, we have*

$$\begin{aligned} z_1(x,t;\lambda) &= \textstyle\int_0^{+\infty}\sin(\lambda(t-\tau))K(x,\tau)d\tau \\ &= |e^{-x\sqrt{i\lambda}}|\sin(\lambda t - x\sqrt{\tfrac{\lambda}{2}}) = e^{-x\sqrt{\frac{\lambda}{2}}}\sin(\lambda t - x\sqrt{\tfrac{\lambda}{2}}). \end{aligned} \tag{14}$$

Proof. Using a trigonometric identity for the sine, and the fact that the kernel $K(x,t)$ in (9) is real, we obtain

$$\begin{aligned}
&\int_0^{+\infty} \sin(\lambda(t-\tau))K(x,\tau)d\tau \\
&= \sin(\lambda t)\int_0^{+\infty} \cos(\lambda\tau)K(x,\tau)d\tau - \cos(\lambda t)\int_0^{+\infty} \sin(\lambda\tau)K(x,\tau)d\tau \\
&= \sin(\lambda t)\mathcal{R}e\left(\int_0^{+\infty} e^{-i\lambda\tau}K(x,\tau)d\tau\right) + \cos(\lambda t)\mathcal{I}m\left(\int_0^{+\infty} e^{-i\lambda\tau}K(x,\tau)d\tau\right).
\end{aligned}$$

Now by the definition of the Laplace transform (10), we get

$$\int_0^{+\infty} e^{-i\lambda\tau}K(x,\tau)d\tau = \mathcal{F}(K(x,\cdot))(i\lambda) = e^{-x\sqrt{i\lambda}} = e^{-x\sqrt{\frac{\lambda}{2}}(1+i)},$$

so that we obtain for the original integral

$$\begin{aligned}
\int_0^{+\infty} \sin(\lambda(t-\tau))K(x,\tau)d\tau &= e^{-x\sqrt{\frac{\lambda}{2}}}(\sin(\lambda t)\cos(x\sqrt{\frac{\lambda}{2}}) - \cos(\lambda t)\sin(x\sqrt{\frac{\lambda}{2}})) \\
&= e^{-x\sqrt{\frac{\lambda}{2}}}\sin(\lambda t - x\sqrt{\frac{\lambda}{2}}),
\end{aligned}$$

which concludes the proof of the lemma. □

We can now prove Theorem 1.

Proof of Theorem 1. By definition of z_1 and z_2 we have

$$e_1^k(0,t) - z_1((2k-1)\frac{L}{\sqrt{\nu}},t;\lambda) = z_2((2k-1)\frac{L}{\sqrt{\nu}},t;\lambda).$$

With a direct estimation, using that the sine is bounded by 1 in modulus, and the definition (9) of the kernel function $K(x,t)$, we obtain

$$\begin{aligned}
|z_2(x,t;\lambda)| &= \left|\int_t^{+\infty} \sin(\lambda(t-\tau))K(x,\tau)d\tau\right| \\
&\leq \int_t^{+\infty} K(x,\tau)d\tau \leq \int_t^{+\infty} \frac{x}{\sqrt{\pi\tau^3}}d\tau = \frac{x}{2\sqrt{\pi t}}.
\end{aligned}$$

Hence for large t, the error $e_1^k(0,t)$ is well approximated by $z_1((2k-1)\frac{L}{\sqrt{\nu}},t;\lambda)$, and using the estimate in Lemma 1 then gives the desired result. □

The next lemma gives an estimate for z_2 for large frequencies λ.

Lemma 2. *For large frequency parameter λ, the function $z_2(x,t;\lambda)$ satisfies*

$$z_2(x,t;\lambda) = -\int_t^{+\infty} \sin(\lambda(t-\tau))K(x,\tau)d\tau = \frac{1}{\lambda}K(x,t) + \mathcal{O}(\frac{1}{\lambda^3}).$$

Proof. Using integration by parts, we obtain

$$\begin{aligned}\int_t^{+\infty} \sin(\lambda(t-\tau))K(x,\tau)d\tau &= -\frac{1}{\lambda}K(x,t) - \frac{1}{\lambda}\int_t^{+\infty} \cos(\lambda(t-\tau))\frac{\partial K}{\partial t}(x,\tau)d\tau \\ &= -\frac{1}{\lambda}K(x,t) - \frac{1}{\lambda^2}\int_t^{+\infty} \sin(\lambda(t-\tau))\frac{\partial^2 K}{\partial t^2}(x,\tau)d\tau \\ &= -\frac{1}{\lambda}K(x,t) + \frac{1}{\lambda^3}\frac{\partial^2 K}{\partial t^2}(x,t) + \mathcal{O}(\frac{1}{\lambda^5}),\end{aligned}$$

which concludes the proof of the lemma. □

We can now prove Theorem 2.

Proof of Theorem 2. The behavior for large λ is a direct application of Lemma 2. We now prove the result for large k. A change of variables gives for $\mu > 0$

$$\int_t^{+\infty} \sin(\lambda(t-\tau))K(x,\tau)d\tau = \int_{\frac{\lambda}{\mu}t}^{+\infty} \sin(\mu(\frac{\lambda}{\mu}t-\tau))x\sqrt{\frac{\lambda}{\mu}}\frac{e^{-\frac{x^2}{4\tau}\frac{\lambda}{\mu}}}{\tau^{3/2}}d\tau,$$

and thus

$$z_2(x,t;\lambda) = z_2(x\sqrt{\frac{\lambda}{\mu}}, \frac{\lambda}{\mu}t; \mu).$$

As a consequence, choosing $\mu = \lambda x^2$, we obtain $z_2(x,t;\lambda) = z_2(1, \frac{t}{x^2}; \lambda x^2)$ and

$$\max_{t\in[0,+\infty)} |z_2(x,t;\lambda)| = \max_{t\in[0,+\infty)} |z_2(1,\frac{t}{x^2};\lambda x^2)| = \max_{t\in[0,+\infty)} |z_2(1,t;\lambda x^2)|.$$

Now using Lemma 2, we obtain for large x that $z_2(1,t;\lambda x^2) \sim \frac{1}{\lambda x^2}K(1,t)$. We also have $\max_{t\in[0,+\infty)} K(1,t) = K(1,\frac{1}{6}) = \frac{3\sqrt{6}}{\sqrt{\pi}}e^{-\frac{3}{2}}$, and assuming that the maximum and the limit can be interchanged, we get

$$\|z_2((2k-1)\frac{L}{\sqrt{\nu}},t;\lambda)\|_{L^\infty(0,+\infty)} \sim \frac{3\sqrt{6}}{\lambda\sqrt{\pi}((2k-1)\frac{L}{\sqrt{\nu}})^2}e^{-\frac{3}{2}}.$$

The last result in the theorem then follows by looking at the ratio between z_2 evaluated at $2k+1$ and $2k-1$. □

We now illustrate the results of Theorem 1 and Theorem 2 numerically. We use for the thermal parameter $\nu = 1$ and set the time horizon to $T = 5$. We consider a finite spatial domain $\Omega := (0,20)$, which we decompose into the two subdomains $\Omega_1 := (0,\beta)$ and $\Omega_2 := (\alpha,20)$ with $\beta = 10$ and $\alpha = 10 - 0.02$, so that the overlap is $L = 0.02$. We use a standard second order finite difference discretization in space, and Backward Euler in time, with space and time steps $\Delta x = \Delta t = \frac{20}{20000} = 10^{-3}$. The initial guess is $e_2^0(\beta,t) = \sin(\lambda t)$, and we will consider several values of λ. In Figure 4 we show the behavior of the error $e_1^k(\alpha,t)$ as a function of the time t for several values of the iteration index k

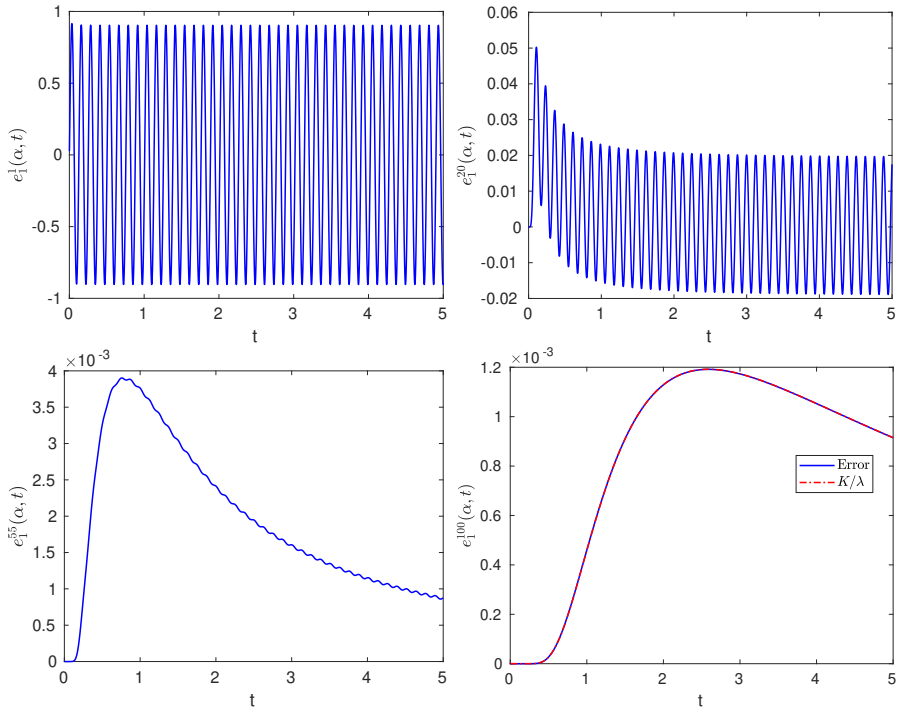

Figure 4: Error $e_1^k(\alpha,t)$ as a function of time t for iteration index $k = 1, 20, 55, 100$ when using a pure sine initial guess for the error $e_2^0(\beta,t) = \sin(50t)$. In the last panel we also added $K((2k-1)L/2,t)/\lambda$ for comparison.

and when $\lambda = 50$. For the first iterations, we see that for large t the error is a sine contracted by $\rho_L(\lambda)$, as shown in Theorem 1, while when k becomes large, the convergence is guided by the function z_2, as we see in the last two panels of Figure 4. In the last panel, we also show that the error $e_1^k(\alpha, t)$ is very close to the scaled kernel $K((2k-1)L/2, t)/\lambda$ for the large iteration number $k = 100$.

In Figure 5 we show the infinity norm of the error as a function of the iteration index k for three values of the frequency λ. In Figure 5 (left) we evaluate the error only on the time interval $(T/2, T)$, i.e. for large time t, and we see that for a substantial number of iterations at the beginning of the Schwarz waveform relaxation algorithm, the convergence is clearly guided by the Fourier convergence factor $\rho_L(\lambda)$, which leads to linear convergence, as in the case of Schwarz applied to the screened Laplace problem. For later iterations however, the bump we observed in Figure 4 (right) becomes dominant for the convergence mechanism of the Schwarz waveform relaxation algorithm, and causes the convergence to be dominated by the term z_2. In Figure 5 (right) we show the error computed on the entire time domain $(0, T)$. We see that again for the first few iterations the convergence is linear, as predicted by the Fourier convergence factor, but then a transition happens and the algorithm clearly converges like predicted by the bump, represented by the kernel function $K(x, t)$.

We next investigate a case where all the frequencies are present: in Figure 6 we show the evolution of the error as a function of the iterations when the initial guess $e_2^0(\beta, t) = g(t)$ is random with values in $(-1, 1)$. Here we chose $T = 30$ as for Figure 1 (right) to better identify the various convergence regimes; the spatial domain is $(-30, 30)$, and we used the mesh size $\Delta x = \Delta t = 0.005$ and overlap $L = 5\Delta x$. We see that the bump represented by the kernel function $K(x, t)$ clearly dominates the convergence for a substantial number of early iterations. Then the algorithm feels the effect of the finite time interval and superlinear convergence sets in, as it was proved in [3] using a heat kernel estimate. We therefore have now a complete understanding of the various convergence phases of Schwarz waveform relaxation applied to the heat equation, and the behavior is quite different from the one suggested by a simple Fourier/Laplace type analysis.

4. Generalization to the advection-reaction-diffusion equation

Our analysis can be generalized to the advection-reaction-diffusion equation with a, c and $\nu > 0$ three real values,

$$\begin{aligned} &\mathcal{L}_{ad} u := \frac{\partial u}{\partial t} + a\frac{\partial u}{\partial x} - \nu\frac{\partial^2 u}{\partial x^2} + cu = f \quad \text{in } \mathbb{R} \times (0, T), \\ &u(\cdot, 0) = u_0 \qquad\qquad\qquad\qquad\qquad\quad \text{in } \mathbb{R}. \end{aligned} \tag{15}$$

The Schwarz waveform relaxation algorithm (6) can be used, simply replacing $\mathcal{L}$ by $\mathcal{L}_{ad}$.

As for the screened Laplace equation and the heat equation, we show in Figure 7 the level sets of the solution of the advection reaction diffusion equation (15) on $\mathbb{R}^+ \times (0, T)$ when $\nu = 1$, $a = 2$, $c = 1$ and the boundary condition is

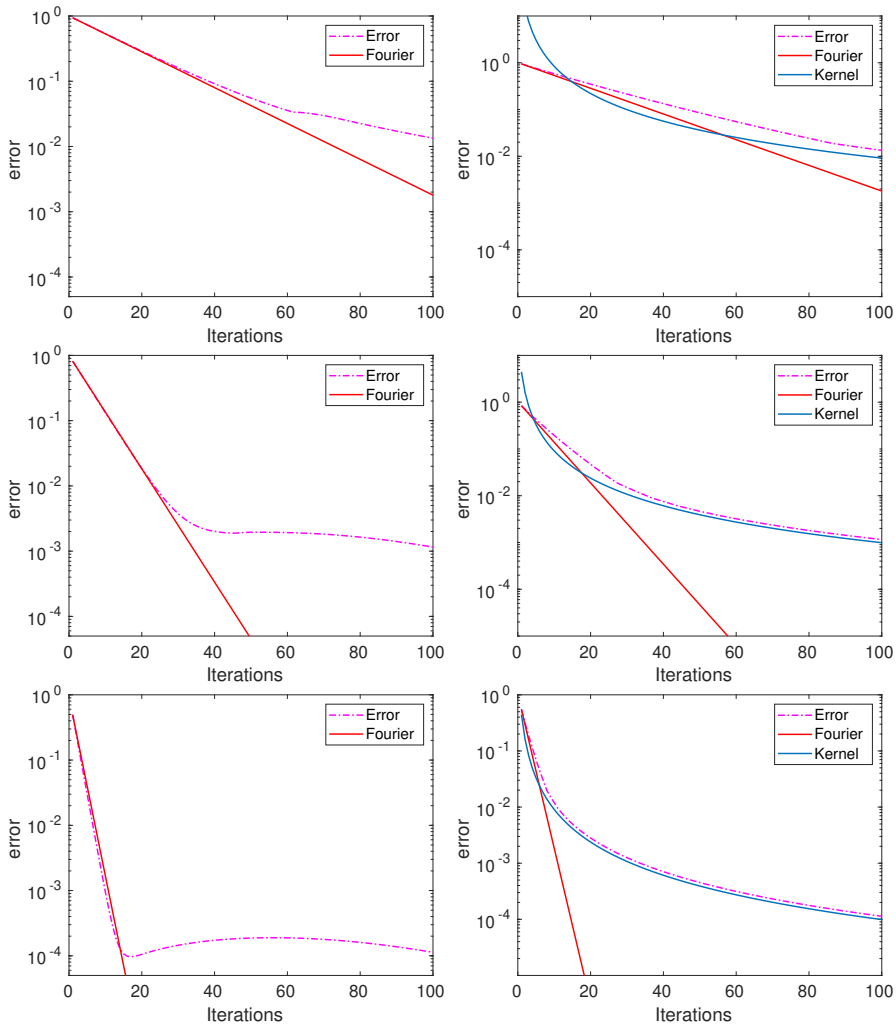

Figure 5: Error $\|e_1^k(\alpha,\cdot)\|_{L^\infty(\frac{T}{2},T)}$ (left) and $\|e_1^k(\alpha,\cdot)\|_{L^\infty(0,T)}$ (right) versus iteration. From top to bottom: $\lambda = 5$, $\lambda = 50$ and $\lambda = 500$.

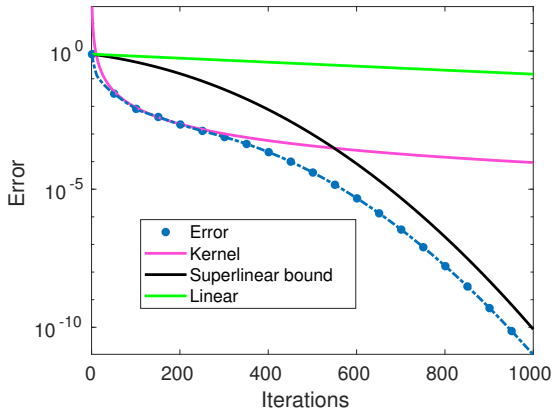

Figure 6: Error $\|e_1^k(\alpha,\cdot)\|_{L^\infty(0,T)}$ versus iteration when the initial guess is random in $(-1,1)$.

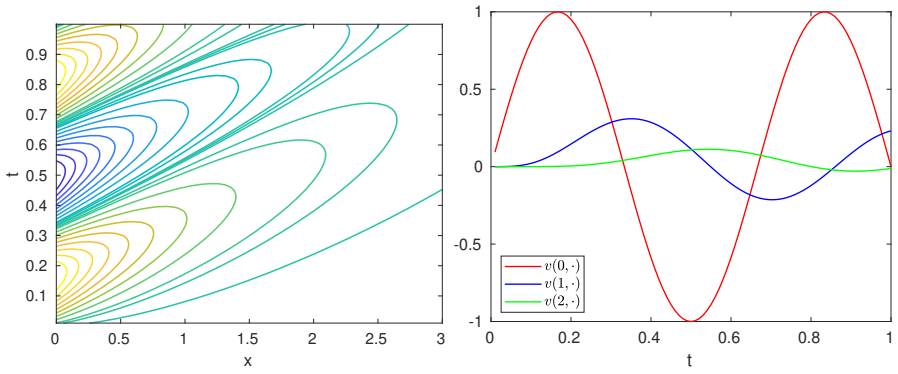

Figure 7: Left: level sets of the solution of the advection-reaction-diffusion equation in the (x,t)-quadrant when $v(0,t) = \sin(3\pi t)$. On the right: slices of the solution at $x = 0$, $x = 1$ and $x = 2$.

$u(0,t) = \sin(3\pi t)$, with zero initial condition. We see a similar pattern as for the heat equation in Figure 3, but the advection reaction diffusion equation has a direction now, namely the advection, in contrast to the heat equation, and thus the useful symmetry argument does not seem to be directly applicable any more.

To study this further, we introduce again the solutions for the errors after a Laplace transform, and obtain for an initial error $e_2^0(L,t) := g(t)$

$$\begin{aligned} \hat{e}_1^k(0,s) &= \hat{g}(s) e^{-\frac{aL}{2\nu}} e^{-(2k-1)\frac{L\delta}{2\nu}}, \\ \hat{e}_2^k(L,s) &= \hat{g}(s) e^{-\frac{kL\delta}{\nu}}, \end{aligned} \tag{16}$$

where $\delta := \sqrt{a^2 + 4\nu(c+s)} = 2\sqrt{\nu}\sqrt{s+A}$, $A := \frac{a^2+4\nu c}{4\nu}$.

Denoting by v the bounded solution of $\mathcal{L}_{ad} v = 0$ on $(0,+\infty) \times (0,+\infty)$ with the initial condition $v(\cdot,0) = 0$ and the boundary condition $v(0,\cdot) = g$, we have in Laplace space $\hat{v}(x,s) = \hat{g}(s) e^{\frac{a-\delta}{2\nu}x}$, and the errors can be written as $\hat{e}_1^k(0,s) = e^{-\frac{a}{\nu}kL} \hat{v}((2k-1)L, s)$ and $\hat{e}_2^k(L,s) = e^{-\frac{a}{\nu}kL} \hat{v}(2kL, s)$, and therefore it still suffices to study the solution v in order to understand the errors e_j^k in the algorithm.

To obtain the back-transforms for the errors in (16), we will use the two following lemmas:

Lemma 3. *Let $x > 0$ and A be two real numbers. We then have*

$$e^{-x\sqrt{s+A}} = \frac{x}{2\sqrt{\pi}} \mathcal{F}(e^{-At} \frac{e^{-\frac{x^2}{4t}}}{t^{3/2}}). \tag{17}$$

Proof. The proof uses the shifting formula of Laplace transforms, $\hat{f}(s+A) = \mathcal{F}(e^{-At} f(t))$ and the definition of the Laplace transform (10). □

Lemma 4. *If $\hat{e}(s) = \hat{g}(s) e^{-x\sqrt{s+A}}$ with $g(t) = \sin(\lambda t)$, then*

$$e(t) = \int_0^t \sin(\lambda(t-\tau)) H(\tau; x, A) d\tau,$$

where now the kernel function is given by

$$H(\tau; x, A) := e^{-A\tau} K(x,\tau) = \frac{x}{2\sqrt{\pi}} e^{-A\tau} \frac{e^{-\frac{x^2}{4\tau}}}{\tau^{3/2}}. \tag{18}$$

Moreover we have

$$\int_0^{+\infty} \sin(\lambda(t-\tau)) H(\tau; x, A) d\tau = |e^{-x\sqrt{i\lambda+A}}| \sin(\lambda t - x\tilde{B}),$$

where $\sqrt{i\lambda + A} = \tilde{A} + i\tilde{B}$, $\tilde{A}$, $\tilde{B} \in \mathbb{R}$.

Proof. Using Lemma 3, we obtain

$$\mathcal{F}(t \to H(t;x,A))(s) = e^{-x\sqrt{s+A}}.$$

Now using similar arguments as in the proof of Theorem 1, we obtain

$$\begin{aligned}
&\int_0^{+\infty} \sin(\lambda(t-\tau))H(\tau;x,A)d\tau \\
&\quad = \sin(\lambda t)\mathcal{R}e(\mathcal{F}(H(\tau;x,A)(i\lambda))) + \cos(\lambda t)\mathcal{I}m(\mathcal{F}(H(\tau;x,A)(i\lambda))) \\
&\quad = \sin(\lambda t)\mathcal{R}e(e^{-x\sqrt{i\lambda+A}}) + \cos(\lambda t)\mathcal{I}m(e^{-x\sqrt{i\lambda+A}}) \\
&\quad = e^{-\tilde{A}x}(\sin(\lambda t)\cos(x\tilde{B}) - \cos(\lambda t)\sin(x\tilde{B})) \\
&\quad = |e^{-x\sqrt{i\lambda+A}}|\sin(\lambda t - x\tilde{B}),
\end{aligned}$$

and the proof is complete. □

Theorem 3. *Let $T = +\infty$. If the Schwarz waveform relaxation algorithm* (6) *for the advection reaction diffusion problem* (15) *is initialized with a pure sine frequency error $e_2^0(L,t) = \sin(\lambda t)$, then we have*

$$\begin{aligned}
e_1^k(0,t) = |\rho_{ad}(\lambda)|^{2k-1}e^{-\frac{aL}{2\nu}}\sin(\lambda t - (2k-1)LG(a,c,\nu,\lambda)) \\
+e^{-\frac{aL}{2\nu}}w_2(t;(2k-1)\tfrac{L}{\sqrt{\nu}},\tfrac{a^2+4\nu c}{4\nu},\lambda),
\end{aligned} \tag{19}$$

where the Fourier convergence factor is given by

$$\rho_{ad}(\lambda) = e^{-\frac{L}{2\nu}\sqrt{a^2+4\nu c+4i\lambda\nu}}, \tag{20}$$

and where G and w_2 are defined by

$$G(a,c,\nu,\lambda) = \frac{1}{2\nu\sqrt{2}}\sqrt{-(a^2+4\nu c) + \sqrt{(a^2+4\nu c)^2 + 16\nu^2\lambda^2}}),$$

and

$$w_2(t;x,A,\lambda) = -\int_t^{+\infty} \sin(\lambda(t-\tau))e^{-A\tau}K(x,\tau)d\tau.$$

As a consequence for large time t we have

$$e_1^k(0,t) = |\rho_{ad}(\lambda)|^{2k-1}e^{-\frac{aL}{2\nu}}\sin(\lambda t - (2k-1)LG(a,c,\nu,\lambda)) + \mathcal{O}(\frac{1}{t^{3/2}}).$$

Furthermore, for large k, we have

$$\frac{\|w_2(\cdot;(2k+1)\frac{L}{\sqrt{\nu}},\frac{a^2+4\nu c}{4\nu},\lambda)\|_{L^\infty(0,+\infty)}}{\|w_2(\cdot;(2k-1)\frac{L}{\sqrt{\nu}},\frac{a^2+4\nu c}{4\nu},\lambda)\|_{L^\infty(0,+\infty)}} \sim \frac{H(t_{k+1};(2k+1)\frac{L}{\sqrt{\nu}},\frac{a^2+4\nu c}{4\nu})}{H(t_k;(2k-1)\frac{L}{\sqrt{\nu}},\frac{a^2+4\nu c}{4\nu})},$$

where $t_k = \frac{\nu}{a^2+4\nu c}(-3 + \sqrt{\frac{(a^2+4\nu c)(2k-1)^2L^2}{\nu^2}+9})$.

Proof. To transform back (16), we apply Lemma 4 with $x = (2k-1)\frac{L}{\sqrt{\nu}}$ and $A = \frac{a^2+4\nu c}{4\nu}$ and we obtain

$$e_1^k(0,t) = e^{-\frac{aL}{2\nu}} \int_0^{+\infty} \sin(\lambda(t-\tau))H(\tau;x,A)d\tau - e^{-\frac{aL}{2\nu}} \int_t^{+\infty} \sin(\lambda(t-\tau))H(\tau;x,A)d\tau.$$

We then get (19) again with Lemma 4 and considering the first integral with $\mathcal{I}m(\sqrt{i\lambda + A}) = \sqrt{\nu}G(a,c,\nu,\lambda)$.

To obtain the behavior of w_2 for large k we use a first integration by parts and get

$$\begin{aligned}
&w_2(t;x,A,\lambda)\\
&= -\int_t^{+\infty} \sin(\lambda(t-\tau))e^{-A\tau}K(x,\tau)d\tau\\
&= -\int_t^{+\infty} \frac{\partial}{\partial\tau}\left((-\frac{A}{A^2+\lambda^2}\sin(\lambda(t-\tau)) + \frac{\lambda}{A^2+\lambda^2}\cos(\lambda(t-\tau)))e^{-A\tau}\right)K(x,\tau)d\tau\\
&= \frac{\lambda}{A^2+\lambda^2}e^{-At}K(x,t) - \frac{A}{A^2+\lambda^2}\int_t^{+\infty} \sin(\lambda(t-\tau))e^{-A\tau}\frac{\partial K}{\partial t}(x,\tau)d\tau\\
&+ \frac{\lambda}{A^2+\lambda^2}\int_t^{+\infty} \cos(\lambda(t-\tau))e^{-A\tau}\frac{\partial K}{\partial t}(x,\tau)d\tau.
\end{aligned}$$

A second integration by parts applied to the second integral gives

$$\begin{aligned}
w_2(t;x,A,\lambda) &= \frac{\lambda}{A^2+\lambda^2}e^{-At}K(x,t) + \frac{A\lambda}{(A^2+\lambda^2)^2}e^{-At}\frac{\partial K}{\partial t}(x,t)\\
&- (\frac{A}{A^2+\lambda^2})^2\int_t^{+\infty} \sin(\lambda(t-\tau))e^{-A\tau}\frac{\partial^2 K}{\partial t^2}(x,\tau)d\tau\\
&+ \frac{A\lambda}{(A^2+\lambda^2)^2}\int_t^{+\infty} \cos(\lambda(t-\tau))e^{-A\tau}\frac{\partial^2 K}{\partial t^2}(x,\tau)d\tau\\
&+ \frac{\lambda}{A^2+\lambda^2}\int_t^{+\infty} \cos(\lambda(t-\tau))e^{-A\tau}\frac{\partial K}{\partial t}(x,\tau)d\tau.
\end{aligned}$$

We use a final integration by parts for the last integral, and find after simplifying

$$\begin{aligned}
w_2(t;x,A,\lambda) &= \frac{\lambda}{A^2+\lambda^2}e^{-At}K(x,t) + \frac{2A\lambda}{(A^2+\lambda^2)^2}e^{-At}\frac{\partial K}{\partial t}(x,t)\\
&- \frac{A^2-\lambda^2}{(A^2+\lambda^2)^2}\int_t^{+\infty} \sin(\lambda(t-\tau))e^{-A\tau}\frac{\partial^2 K}{\partial t^2}(x,\tau)d\tau\\
&+ \frac{2A\lambda}{(A^2+\lambda^2)^2}\int_t^{+\infty} \cos(\lambda(t-\tau))e^{-A\tau}\frac{\partial^2 K}{\partial t^2}(x,\tau)d\tau.
\end{aligned}$$

We now use for a $\mu > 0$ the change of variables $w_2(t;x,A,\lambda) = w_2(\frac{\lambda}{\mu}t; \sqrt{\frac{\lambda}{\mu}}x, A\frac{\mu}{\lambda}, \mu)$, and with $\mu = \lambda x^2$ and we obtain

$$\max_{t\in[0,+\infty)} |w_2(t;x,A,\lambda)| = \max_{t\in[0,+\infty)} |w_2(\frac{t}{x^2};1,Ax^2,\lambda x^2)| = \max_{t\in[0,+\infty)} |w_2(t;1,Ax^2,\lambda x^2)|.$$

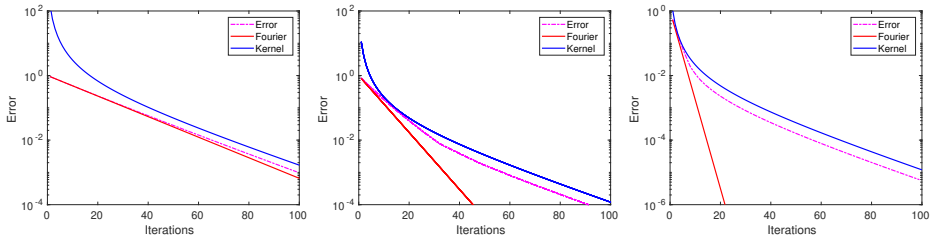

Figure 8: Advection-reaction-diffusion equation: error $\|e_1^k(\alpha,\cdot)\|_{L^\infty(0,T)}$ versus iteration. From left to right: $\lambda = 5$, $\lambda = 50$ and $\lambda = 500$.

However from the previous computations, for large x we have

$$w_2(t;1,Ax^2,\lambda x^2) \sim \frac{\lambda}{x^2(A^2+\lambda^2)} e^{-Ax^2 t} K(1,t).$$

Now, since $\max_{t\geq 0} e^{-Ax^2 t} K(1,t) = e^{-At_x} K(1,\frac{t_x}{x^2})$ with $t_x = \frac{1}{4A}(-3+\sqrt{4Ax^2+9})$, and assuming that the maximum and limit can be interchanged, we conclude that for large x

$$\|w_2(\cdot;1,Ax^2,\lambda x^2)\|_{L^\infty(0,+\infty)} \sim \frac{\lambda}{x^2(A^2+\lambda^2)} e^{-At_x} K(1,\frac{t_x}{x^2}) = \frac{\lambda}{(A^2+\lambda^2)} e^{-At_x} K(x,t_x),$$

which concludes the proof. □

In Figure 8 we show the evolution of the error as a function of the iterations. Here the spatial domains are $\Omega := (0,20)$, $\Omega_1 := (0,10)$, $\Omega_2 := (9.98,20)$ and $T = 5$, $\nu = 1$, $a = 2$, $c = 1$, the spatial and time discretization parameters are $\Delta x = \Delta t = 10^{-3}$ and the overlap is again $L = 0.02$. As for the heat equation, the first iterations are following the Fourier convergence factor whereas for larger iteration numbers the term in the kernel function H dictates the behavior of the convergence.

5. Conclusion

Our work started by the observation that, even though classical Fourier analysis leads to very similar convergence factors, Schwarz waveform relaxation applied to evolution problems shows a rather different convergence behavior compared to Schwarz applied to steady problems, and in fact the Fourier analysis result for Schwarz waveform relaxation never really predicts well the convergence when applied to a heat equation. We then presented a new Fourier kernel analysis for Schwarz waveform relaxation methods which can explain this different convergence behavior, and shows that Fourier analysis in time is different. Our analysis is based on a very useful new symmetry argument, which naturally leads to the iterated kernel estimates we needed, and we showed how to extend these results to advection reaction diffusion problems.

Our main motivation for this work is however to go a step further: the convergence of classical Schwarz and Schwarz waveform relaxation methods can be greatly enhanced by changing the Dirichlet transmission conditions to Robin or Ventcell transmission conditions, leading to optimized variants of these algorithms that converge often orders of magnitudes faster than when using classical transmission conditions [22, 7]. The optimization in these algorithms is based on the Fourier convergence factor, and while this is justified for large times t in the Schwarz waveform relaxation method, it is not for short time t. The present analysis here opens up a new way for the optimization of such transmission conditions in the time dependent case, which turns out to be substantially harder without our new insight [24], and is the focus of future work.

Acknowledgements: This research was supported by the Swiss National Science Foundation.

References

[1] B. F. Smith, P. E. Bjørstad, W. Gropp, Domain Decomposition: Parallel Multilevel Methods for Elliptic Partial Differential Equations, Cambridge University Press, 1996.

[2] M. J. Gander, H. Zhao, Overlapping Schwarz waveform relaxation for parabolic problems in higher dimension, in: A. Handlovičová, M. Komorníkova, K. Mikula (Eds.), Proceedings of Algoritmy 14, Slovak Technical University, 1997, pp. 42–51.

[3] M. J. Gander, A. M. Stuart, Space time continuous analysis of waveform relaxation for the heat equation, SIAM J. 19 (1998) 2014–2031.

[4] A. Quarteroni, A. Valli, Domain decomposition methods for partial differential equations, Oxford University Press, 1999.

[5] M. J. Gander, L. Halpern, F. Nataf, Optimal Schwarz waveform relaxation for the one dimensional wave equation, SIAM Journal of Numerical Analysis 41 (5) (2003) 1643–1681.

[6] A. Toselli, O. Widlund, Domain decomposition methods-algorithms and theory, Vol. 34, Springer Science & Business Media, 2004.

[7] M. J. Gander, L. Halpern, Optimized Schwarz waveform relaxation methods for advection reaction diffusion problems, SIAM J. Numer. Anal. 45 (2) (2007) 666–697.

[8] D. Bennequin, M. Gander, L. Halpern, A homographic best approximation problem with application to optimized schwarz waveform relaxation, Math. of Comp. 78 (2009) 75–90.

[9] V. Dolean, P. Jolivet, F. Nataf, An introduction to domain decomposition methods: algorithms, theory, and parallel implementation, SIAM, 2015.

[10] D. Bennequin, M. J. Gander, L. Gouarin, L. Halpern, Optimized Schwarz waveform relaxation for advection reaction diffusion equations in two dimensions, Numerische Mathematik 134 (3) (2016) 513–567.

[11] H. A. Schwarz, Über einen grenzübergang durch alternierendes verfahren, ierteljahrsschrift der Naturforschenden Gesellschaft in Zürich 15 (1870) 272–286.

[12] K. Miller, Numerical analogs to the Schwarz alternating procedure, Numer. Math. 7 (1965) 91–103.

[13] P.-L. Lions, On the Schwarz alternating method. I., in: R. Glowinski, G. H. Golub, G. A. Meurant, J. Périaux (Eds.), First International Symposium on Domain Decomposition Methods for Partial Differential Equations, SIAM, Philadelphia, PA, 1988, pp. 1–42.

[14] M. Dryja, O. B. Widlund, An additive variant of the Schwarz alternating method for the case of many subregions, Tech. Rep. 339, also Ultracomputer Note 131, Department of Computer Science, Courant Institute (1987).

[15] M. J. Gander, Schwarz methods over the course of time, Electronic Transactions on Numerical Analysis 31 (5) (2008) 228–255.

[16] M. J. Gander, G. Wanner, The origins of the alternating Schwarz method, in: J. Erhel, M. J. Gander, L. Halpern, G. Pichot, T. Sassi, O. Widlund (Eds.), Domain Decomposition Methods in Science and Engineering XXI, Springer International Publishing, Cham, 2014, pp. 487–495.

[17] E. Lelarasmee, A. E. Ruehli, A. L. Sangiovanni-Vincentelli, The waveform relaxation method for time-domain analysis of large scale integrated circuits, IEEE Trans. on CAD of IC and Syst. 1 (1982) 131–145.

[18] M. J. Gander, Overlapping Schwarz for parabolic problems, in: P. E. Bjørstad, M. Espedal, D. Keyes (Eds.), Ninth International Conference on Domain Decomposition Methods, ddm.org, 1997, pp. 97–104.

[19] M. J. Gander, L. Halpern, F. Nataf, Optimal convergence for overlapping and non-overlapping Schwarz waveform relaxation, in: Eleventh International Conference on Domain Decomposition Methods (London, 1998), DDM.org, Augsburg, 1999, pp. 27–36.

[20] M. J. Gander, L. Halpern, F. Nataf, Optimized Schwarz methods, in: T. Chan, T. Kako, H. Kawarada, O. Pironneau (Eds.), Twelfth International Conference on Domain Decomposition Methods, Chiba, Japan, Domain Decomposition Press, Bergen, 2001, pp. 15–28.

[21] C. Japhet, Optimized Krylov-Ventcell method. Application to convection-diffusion problems, in: P. E. Bjørstad, M. S. Espedal, D. E. Keyes (Eds.), Proceedings of the 9th international conference on domain decomposition methods, ddm.org, 1998, pp. 382–389.

[22] M. J. Gander, Optimized Schwarz methods, SIAM J. Numer. Anal. 44 (2) (2006) 699–731.

[23] E. Giladi, H. B. Keller, Space time domain decomposition for parabolic problems, Numerische Mathematik 93 (2) (2002) 279–313.

[24] Y. Courvoisier, M. J. Gander, Optimization of Schwarz waveform relaxation over short time windows, Numerical Algorithms 64 (2) (2013) 221–243.

[25] M. J. Gander, L. Halpern, Absorbing boundary conditions for the wave equation and parallel computing, Math. of Comp. 74 (249) (2004) 153–176.

[26] M. J. Gander, 50 years of time parallel time integration, in: T. Carraro, M. Geiger, S. Körkel, R. Rannacher (Eds.), Multiple Shooting and Time Domain Decomposition, Springer, 2015, pp. 69–114.

[27] B. W. Ong, J. B. Schroder, Applications of time parallelization, Computing and Visualization in Science 23 (1) (2020) 1–15.

[28] M. J. Gander, L. Halpern, Méthodes de relaxation d'ondes pour l'équation de la chaleur en dimension 1, C.R. Acad. Sci. Paris, Série I 336 (6) (2003) 519–524.